

A Novel Ultra-Lightweight Multiband Rectenna on Paper for RF Energy Harvesting in the Next Generation LTE Bands

Valentina Palazzi, *Student Member, IEEE*, Jimmy Hester, *Student Member, IEEE*, Jo Bitto, *Student Member, IEEE*, Federico Alimenti, *Senior Member, IEEE*, Christos Kalialakis, *Senior Member, IEEE*, Ana Collado, *Senior Member, IEEE*, Paolo Mezzanotte, *Member, IEEE*, Apostolos Georgiadis, *Senior Member, IEEE*, Luca Roselli, *Senior Member, IEEE*, and Manos M. Tentzeris, *Fellow, IEEE*

Abstract—This paper introduces a novel compact ultra-lightweight multiband RF energy harvester fabricated on a paper substrate. The proposed rectenna is designed to operate in all recently released LTE bands (range 0.79–0.96 GHz; 1.71–2.17 GHz; and 2.5–2.69 GHz). High compactness and ease of integration between antenna and rectifier are achieved by using a topology of nested annular slots. The proposed rectifier features an RF-to-dc conversion efficiency in the range of 5%–16% for an available input power of -20 dBm in all bands of interest, which increases up to 11%–30% at -15 dBm. The rectenna has been finally tested both in laboratory and in realistic scenarios featuring a superior performance to other state-of-the-art RF harvesters on flexible substrates.

Index Terms—Broadband antennas, conformal antennas, copper adhesive laminate, energy harvesting, flexible electronics, Internet of Everything, Internet of Things (IoT), multiband rectifier, rectennas, slot antennas.

I. INTRODUCTION

IN THE near future, an explosion of the number of devices connected to the Internet is foreseen, which will impose tremendous challenges both in terms of spectrum and power supply [1]–[4]. On the one hand, new communication protocols and wider bandwidths will be released to manage this huge number of heterogeneous users (both humans and machines), with different levels of intelligence and needs [5]. On the other hand, according to the emerging

Internet of Things (IoT) paradigm, electronic apparatuses will be deployed almost everywhere. The next generation of sensors and circuits will be literally embedded in the items, so their maintenance will be hindered by the fact that they will be difficult to reach or even to localize. This means that the battery replacement will be difficult or even impractical, so, in most of the cases, batteryless devices will be the only option. Additionally, these devices have to be conformal to the hosting objects both in terms of shape and cost, while the environmental impact of these distributed and ubiquitous electronics should be minimized in order not to increase the pollution risks and cause a worsening of the quality of human life.

For these reasons, it is important to avoid the traditional battery and to find new efficient and reliable ways to power the circuits from ambient RF sources, both exploiting already available resources through wireless energy harvesting and enabling the intentional wireless power transferring, so as to make them robust and autonomous.

To this end, research is focusing on both the development of low-power sensors and energy harvesting to produce autonomous wirelessly interconnected smart nodes [6]. State-of-the-art dc/dc converters are able to operate for input voltages as low as 70 mV [7], thus thoroughly reducing the amount of energy required for electronics. Thanks to this trend, ambient RF energy harvesting is becoming ever more appealing among the different forms of energy harvesting (e.g., solar, mechanical, and thermal). So far, the scarcity of the available power density has been its main drawback, but both the development of lower power and lower voltage circuits and the increasing number of wireless applications, which in the future will lead to a dramatic increase of the ambient RF energy, are concurrently bridging the gap.

In this scenario, broadband rectennas are the most suitable solutions to realize reliable power supply [8], since they are able to harness a larger part of the available spectrum; plus, the harvester should be easily mounted on commonly used objects, so it is necessary that they are lightweight and conformal.

Recently, numerous high-performing broadband and multiband rectennas have been proposed (see [9]–[15]), which are able to take advantage of the simultaneous presence of

Manuscript received March 25, 2017; revised May 25, 2017; accepted May 30, 2017. Date of publication July 20, 2017; date of current version January 4, 2018. This work was supported in part by the DTRA, in part by the NSF, in part by the SRC, and in part by Texas Instruments Incorporated. The work of C. Kalialakis was supported by the European Union Horizon 2020 Research and Innovation Programme through the Marie Skłodowska-Curie Grant Agreement under Grant 654734. (*Corresponding author: Valentina Palazzi.*)

V. Palazzi, F. Alimenti, P. Mezzanotte, and L. Roselli are with the Department of Engineering, University of Perugia, 06125 Perugia, Italy (e-mail: valentina.palazzi@studenti.unipg.it).

J. Hester, J. Bitto, and M. M. Tentzeris are with the School of Electrical and Computer Engineering, Georgia Institute of Technology, Atlanta, GA 30309 USA.

C. Kalialakis is with the Centre Tecnològic de Telecomunicacions de Catalunya, 08860 Barcelona, Spain.

A. Collado and A. Georgiadis are with the Institute of Sensors, Signals and Systems, Heriot-Watt University, Edinburgh EH14 4AS, U.K.

Color versions of one or more of the figures in this paper are available online at <http://ieeexplore.ieee.org>.

Digital Object Identifier 10.1109/TMTT.2017.2721399

TABLE I
RELEASED LTE BANDS (EUROPE)

Band	Uplink (MHz)	Downlink (MHz)	Alias
1	1920-1980	2110-2170	UMTS, IMT2100
3	1710-1785	1805-1880	DCS1800
7	2500-2570	2620-2690	IMT-E2600
8	880-915	925-960	GSM900, EGSM900
20	832-862	791-821	EU Digital Dividend 800 MHz
33	1900-1920	1900-1920	pre IMT
34	2010-2025	2010-2025	IMT
38	2570-2620	2570-2620	IMT-E2600 (duplex spacing)

RF power at different frequencies. An in-depth analysis of the rectifier architectures and operating principles was conducted as well, aiming at improving specific properties of the harvesting circuits, such as their sensitivity [14], bandwidth [16], and operating power range [17]. However, further improvements are needed in terms of compactness and conformability to achieve truly practical and scalable solutions.

This paper is a substantial expansion of [18] and [19]. In the previous works, a single band rectenna was designed and demonstrated. Here, both the antenna and the rectifier have been enhanced in order to allow for multiband operation. Furthermore, a compact printed module integrating the proposed new antenna is demonstrated. In the end, a novel ultracompact multiband rectenna is presented, able to harvest power from all released LTE bands.

This paper is organized as follows. Section II presents the system-level design of the multiband rectenna. Section III describes the low-cost fabrication technology utilized for the rectenna prototype. Sections IV and V describe the design procedure of the proposed harvester for the antenna and the rectifier, respectively. Results discussing the performance of the rectenna in various representative harvesting scenarios are given in Section VI. The conclusions are drawn in Section VII.

II. SYSTEM LEVEL DESIGN

The proposed rectenna is aimed at harvesting energy from all new bands released by the Third Generation Partnership Project (3GPP) [20], [21], both in uplink and in downlink. A list of the bands adopted in Europe is reported in Table I. It has been noticed that all these bands can be divided into two groups well separated in frequency: bands 8 and 20 on the one hand, which occupy the range from 790 to 960 MHz, and all others on the other hand, which extend from 1710 to 2690 MHz.

Therefore, an approach based on two antennas has been developed instead of a single broadband rectenna. The rectenna block diagram is reported in Fig. 1. The idea is to use a relatively narrowband antenna tuned around 900 MHz and a broadband one which is able to gather energy from

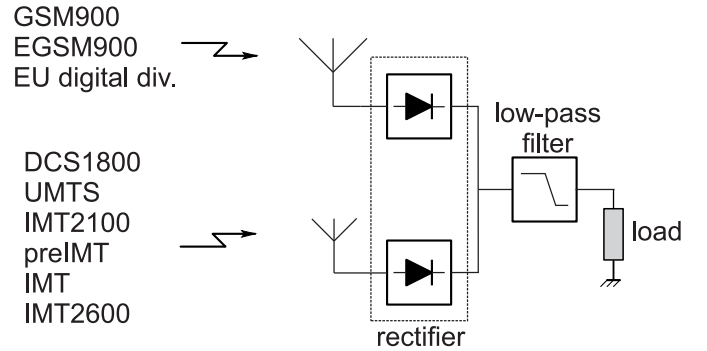


Fig. 1. Architecture of the proposed multiband rectenna.

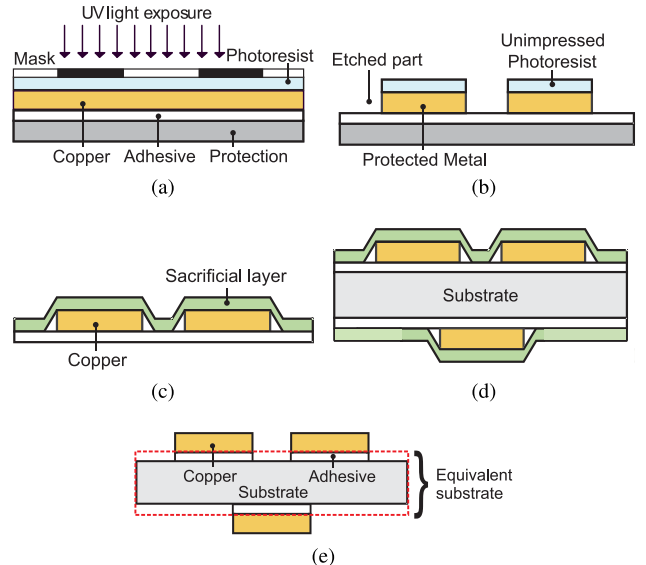


Fig. 2. Adhesive copper laminate technology: fabrication steps. (a) Deposition and selective exposure of photoresist to UV light through a mask. (b) Wet etching of copper. (c) Introduction of a sacrificial layer on the copper side and removal of the protection of the adhesive layer. (d) Transferring of the etched traces to both sides of the substrate. (e) Removal of the sacrificial layer.

frequencies between 1.71 and 2.69 GHz. Both antennas are connected to two separate rectifiers and then their outputs are summed with a dc combining technique. Finally, an RC low-pass filter isolates the dc component, which can be utilized by practical loads (a low-power sensor, a dc/dc converter, and so on).

Thanks to this approach, the bandwidth requirements for both the antenna and the rectifier are less demanding, thus allowing for a reduction in the complexity of each circuit block. On the other hand, the number of blocks is increased. So, in order not to end up with an increased rectenna area, it is essential to choose the most suitable technology and guarantee a compact arrangement of the utilized components.

III. ADHESIVE COPPER LAMINATE TECHNOLOGY

The whole circuit has been manufactured on a paper substrate using the adhesive copper laminate technology described in detail in [22]. The main steps of this technology are reported in Fig. 2. It relies on a copper adhesive tape shaped by a photolithographic process [see Fig. 2(a) and (b)] and then transferred to the paper substrate by means of a sacrificial layer [Fig. 2(c)]. Since in this paper a double layer structure

is needed, the two layers are processed separately by using two different pieces of copper tape that are then attached to the two sides of the substrate [Fig. 2(d) and (e)] and manually aligned by means of alignment marks. The latter process is estimated to feature a misalignment tolerance of about 1 mm, which can be considered acceptable in the low-GHz range. In the case of a simple microstrip structure, a slab of copper tape is attached to the bottom side of the substrate so as to obtain a ground plane.

The advantages of the adopted technique with respect to other emerging ones, such as ink-jet printing [23], are higher metal conductivity ($\sigma = 5.8 \times 10^7$ S/m), the possibility to solder surface mount components by means of conventional eutectic alloy while eliminating curing steps, and compatibility with the Printed Circuit Board fabrication equipment. The price to pay for this is the presence of a photolithographic step that makes this technique not fully additive.

In this context, the paper substrate has been chosen for its unique properties of being lightweight, flexible, biodegradable, and intrinsically inexpensive [24], as well as for being an example of unconventional material in full compliance with the IoT paradigm that requires electronic technologies to be as compliant as possible with material or materials in common objects. The electrical parameters of the adopted substrate, which is a photopaper from Mitsubishi Electric (model CK-D715), are quoted in [25]. The equivalent composite substrate, including both the paper substrate and the glue layers interposed between each layer of copper and paper, features a permittivity of 2.55, a loss tangent equal to 0.05, and a thickness of 0.37 mm. Despite the fact that the high losses of the substrate represent a substantial limitation to the circuit performance, especially for the rectifier (see Section V), this paper introduces an ultralow-cost solution and can be considered as a proof-of-concept demonstration of the feasibility of autonomous wireless sensor nodes on almost every kind of material.

IV. ANTENNA DESIGN

The proposed antenna consists of two annular slots nested one inside the other, according to a technique already demonstrated in [26]. The antenna layout is shown in Fig. 3 and its design was carried out by means of Computer Simulation Technology Studio suite. The antenna input ports are marked with “Port1” and “Port2.”

Since the antennas are substantially etched out from the ground plane, they do not add weight to the structure and are compatible with substrates as thin as a sheet of paper. Moreover, slot antennas feature a relatively wide impedance bandwidth due to their low quality factor (see [27]) and, thanks to the exponential decrease of the current density at the borders of the slots, the metal, which surrounds the slots, can be exploited as the ground plane for the circuitry placed on the other side, thus allowing an easy integration between the antenna and the rectifier.

The outer antenna is the tapered annular slot used and analyzed in [18]. The slot, tuned to the band 790–960 MHz, is the result of the intersection of an ellipse and a circle and features a maximum and minimum width of 8.25 and 0.75 mm,

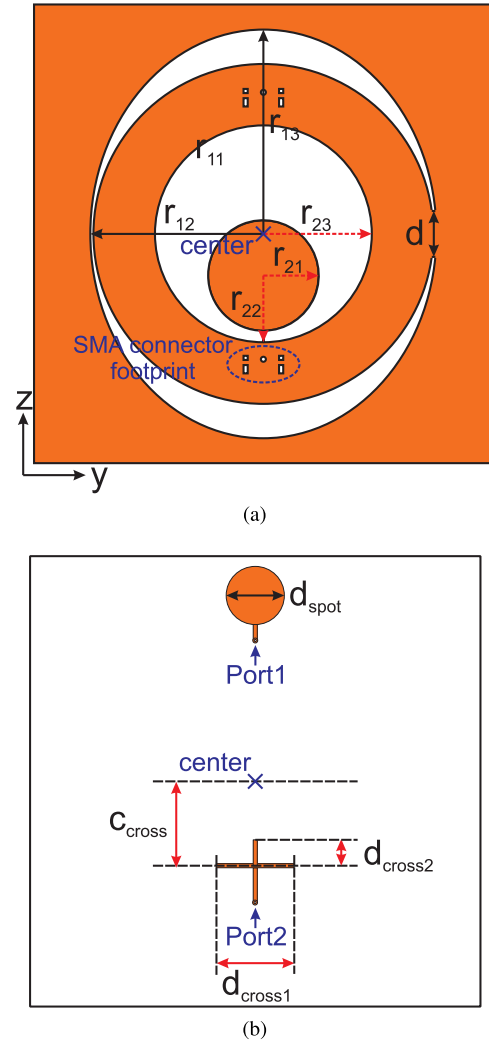


Fig. 3. Layout of the antenna prototype. (a) Top side. (b) Bottom side. Active area: 11×11 cm². The main parameters of the antenna topology are: $r_{11} = 40.75$ mm, $r_{12} = 41.5$ mm, $r_{13} = 49$ mm, $d = 11$ mm, and $d_{\text{spot}} = 14.2$ mm for the first antenna; $r_{21} = 13.24$ mm, $r_{22} = 15.99$ mm, $r_{23} = 26$ mm, $d_{\text{cross1}} = 19$ mm, $d_{\text{cross2}} = 6$ mm, and $c_{\text{cross}} = 21$ mm for the second antenna.

respectively. The antenna is fed by means of a proximity coupled microstrip line terminating on a circular stub introduced to match the antenna to a $50\text{-}\Omega$ impedance, as shown in Fig. 3(b) (Port1). Since the annular slot features a length equal to λ_g , i.e., the guided wavelength in slot technology at the central frequency, the magnitude of the electric field across the slot features a maximum at the feeding point and at its symmetric point (where the slot width is maximum as well), whereas it is ideally null at the antisymmetric points (approximately where the slot width is minimum). As a consequence, the latter two points can be viewed as virtual grounds and it is possible to replace one of them by means of a real short (marked with “d” in Fig. 3) at the expense of an increased cross-polar component [28]. Fig. 4 reports the very minor change in the distribution of the electric field across the slot due to the physical short-circuited connection to the right large ground. On the other hand, this short allows a microstrip line to be placed in a cross configuration below this slot using the metal sheet as ground plane, thus making

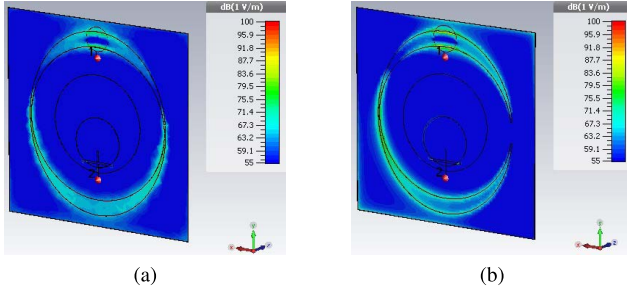


Fig. 4. Electric field distribution at 900 MHz for the outer slot (a) without and (b) with a short-circuit connection to the right large ground.

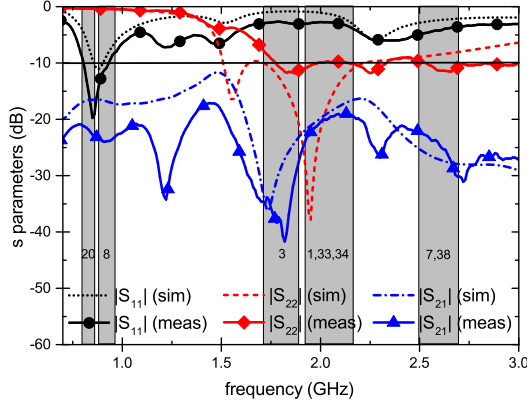


Fig. 5. Scattering parameters of the proposed antenna topology: simulations (solid line) and measurements (dashed line). The bands of interest are marked with gray stripes and their number is reported at the bottom of each stripe.

it possible to arrange circuit components both on the interior and the exterior metal surface of the outer slot.

The inner antenna is a broadband annular slot with a cross-shaped feed line [29]. It consists of a circular slot, a circular patch radiator, which is offset with respect to the slot center, and a proximity-coupled cross-shaped feed line, which also in this case is optimized to obtain a good impedance matching to $50\text{-}\Omega$ throughout the whole band of interest (1.71–2.69 GHz). All relevant parameters of the antenna are reported in Fig. 3.

Fig. 5 shows a comparison between the simulated and measured scattering parameters of the proposed antenna topology. Number “1” refers to the outer slot, while number “2” is linked to the inner slot, according to the port numeration reported in Fig. 3. The bands involved in the design are marked with gray rectangles. A good matching can be noticed in all bands with the exception of the frequency range on the right part of band 8 and on the left part of band 3. The slight mismatch is on the order of 1–2 dB. Slight discrepancies between simulations and measurements are due to fabrication tolerances. Moreover, the mutual coupling is below -19 dB in all frequencies of interest.

Finally, an estimation of the maximum realized gain of both antennas (linear polarization), which occurs in broadside direction, has been reported (see Fig. 6). The first antenna features a gain of 1.3 dBi at 900 MHz and its maximum gain around 2.3 dBi is achieved at 940 MHz, whereas the second antenna features a gain varying between 4 and 6 dBi in

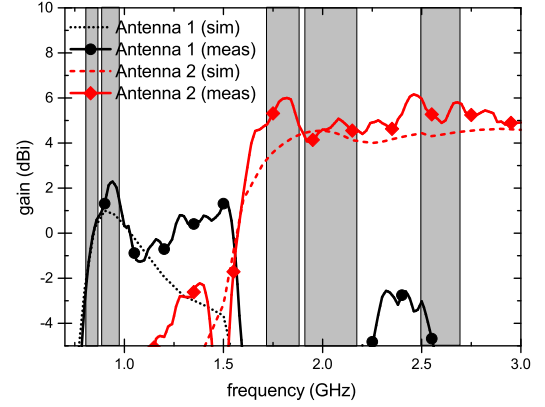


Fig. 6. Measured and simulated gain of the proposed antenna topology.

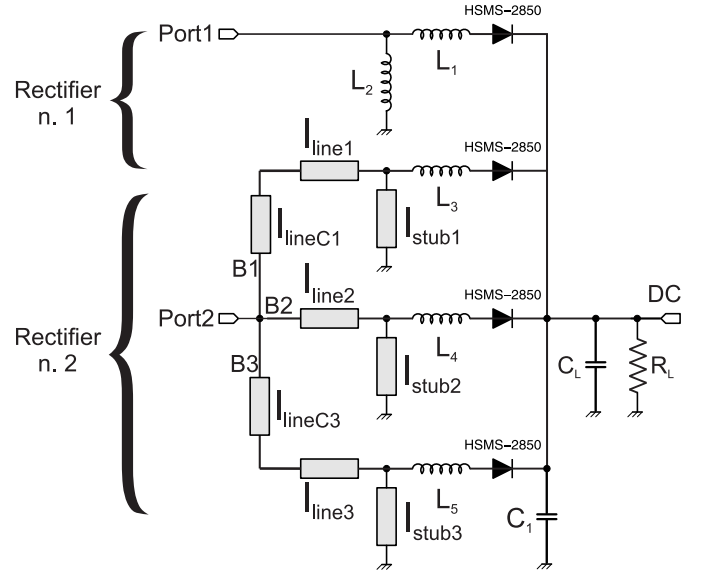


Fig. 7. Schematic of the multiband rectifier. The main circuit parameters are: $L_1 = 47$ nH, $L_2 = 27$ nH, $L_3 = 10$ nH, $L_4 = 8.7$ nH, $L_5 = 4.7$ nH, $l_{\text{stub1}} = 9.1$ mm, $l_{\text{stub2}} = 6.9$ mm, $l_{\text{stub3}} = 5.9$ mm, $w_{\text{stub}} = 0.4$ mm, $l_{\text{lineC1}} = 6.5$ mm, $l_{\text{line1}} = 11$ mm, $l_{\text{line2}} = 13$ mm, $l_{\text{lineC3}} = 4.25$ mm, $l_{\text{line3}} = 11$ mm, $w_{\text{line}} = 1$ mm, $C_1 = 100$ pF, $C_L = 100$ pF, and $R_L = 3$ k Ω .

the band of interest. Antenna #1 features a half-power beamwidth (HPBW) of around 108° in the xy plane and 81° in the xz plane at 900 MHz, whereas antenna #2 shows the HPBW of 78° and 78.5° in the xy plane, and 71° and 63° in the xz plane at 1.8 and 2.6 GHz, respectively.

V. RECTIFIER DESIGN

The design of the rectifier has been carried out with the aim of achieving a good balance among circuit complexity, number of utilized surface mount components, and low-power performance, to be consistent with the inexpensive nature of the adopted substrate.

The schematic of the proposed rectifier is shown in Fig. 7. The circuit parameters have been optimized to achieve the maximum RF-to-dc conversion efficiency for available input power levels ranged between -20 and -15 dBm. The design has been carried out by means of the Advanced Design System suite.

As anticipated in Fig. 1, each antenna is connected to its own rectifier. Due to its relatively small bandwidth (19.3% around 880 MHz), the first rectifier (“rectifier #1” in Fig. 1) was realized with a simple envelope detector. On the other hand, this configuration was impractical for the second rectifier (“rectifier #2”). In fact, because of the frequency-dependent input impedance of the diode and the limited bandwidth of common compact matching networks, it was very hard to achieve a reasonable large-signal input matching all over the band (45% around 2.2 GHz), which is essential to guarantee the maximum power transfer to the load. Examples of multiband single-branch rectifiers have been provided in the literature (see [14], [17], [30], [31]), but such approaches are not able to guarantee the coverage over the intended broad frequency band, while allowing for low-power operation. So, in order to achieve a high RF-to-dc conversion efficiency of the rectifier throughout the band, it has been chosen to connect three envelope detectors in parallel, in such a way that each of them operates in a narrower band, according to the approach reported in [12], effectively synthesizing the aggregate band. Each branch, labeled with “B1,” “B2,” and “B3” in Fig. 7, has been tuned around 1.8, 2.05, and 2.6 GHz, respectively. By optimizing each branch of the rectifier, it is possible to fine-tune its conversion efficiency so as to achieve a local maximum in each subband of interest. To make the optimization process as accurate as possible, the S-parameter files provided for the lumped inductors by the manufacturer were introduced in the Advanced Design System schematic (the selected inductors belong to the Coilcraft 0603HP series).

Each utilized envelope detector is based on a series-connected HSMS2850 low-barrier Schottky diode from Avago, which is suitable for operation in the μW range [32]. Each diode is connected to an input matching network, consisting of an L-type impedance transformer, aimed at converting the input impedance of the antenna (around $50\ \Omega$) to the conjugate of the large-signal input impedance of the diode (see [33]). Unlike in [19], here, some transmission line sections have been replaced by lumped (Coilcraft) components. In fact, it has been observed that the utilized rectifier topology is particularly sensitive to the losses of the line which connects the diode to the stub, since in this section, there is a higher voltage drop (this is actually the aim of the transformer). It was observed that the Coilcraft lumped components are less lossy for the inductance levels of interest in the circuit, as shown in Fig. 8. Simulations were conducted, considering both the S-parameter files of the inductors provided by Coilcraft and the high-impedance microstrip lines connected to ground. The technological pitch of 0.2 mm was chosen for the linewidth. The simulations were performed for both the smallest and the highest inductance values utilized in the rectifier, and in both cases the superiority of the Coilcraft components is noticeable, although this effect is more prominent for the 47-nH inductance. In the first rectifier, the stub has been replaced as well by an inductance due to its low frequency of operation, to reduce the circuit size.

In addition to “lineC1” and “lineC3,” introduced for the sake of feasibility, three transmission line sections (“line1,” “line2,” and “line3” in Fig. 7) have been added to the three branches of

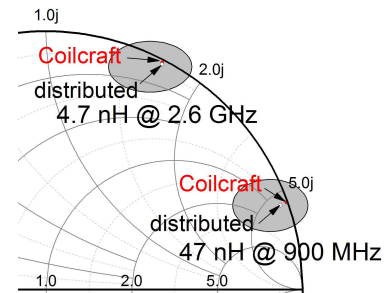


Fig. 8. Inductance implementation: study of the losses related to lumped (Coilcraft) and distributed inductors on paper substrate.

the second rectifier in order to rotate the input impedance of each branch, so that the frequencies outside the operating sub-band feature a high impedance. On the contrary, the operating center frequency of each branch is only marginally affected by its respective line section, since the circuit is designed in such a way that the input impedance at this frequency is approximately located at the center of the Smith chart.

The main idea is to allow each frequency to enter predominantly the branch which is optimized to convert it, thus reducing the consequent loss of power. Fig. 9 reports the input reflection coefficient of each branch of the second rectifier with and without the respective input transmission line sections (“line1,” “line2,” and “line3” are mentioned as “input line” in Fig. 9), whereas Fig. 10 shows the transmission coefficient between Port2 and each branch of the second rectifier. All reported results were calculated for the design power level of $-15\ \text{dBm}$. The addition of these lines was shown to improve the transmission coefficient by up to 4 dB for each branch of the rectifier and for all frequencies of interest. This approach is analogous to that applied to frequency division multiplexers and, although suboptimal for branches B1 and B3 (only one external band can be rotated to open), it eliminates the need to implement high-order bandpass filters [12].

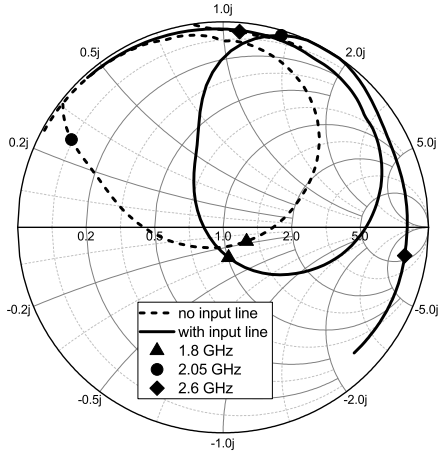
Finally, all branches were connected to a single RC filter, with the exception of the last branch that was tuned to 2.6 GHz, where an additional capacitor was introduced in order to minimize interferences among detectors. The load, equal to $3\ \text{k}\Omega$, was a parameter of the rectifier optimization (see Fig. 17).

In the end, the whole multiband on-paper rectifier was realized with four diodes, five inductors, two capacitors, and the load.

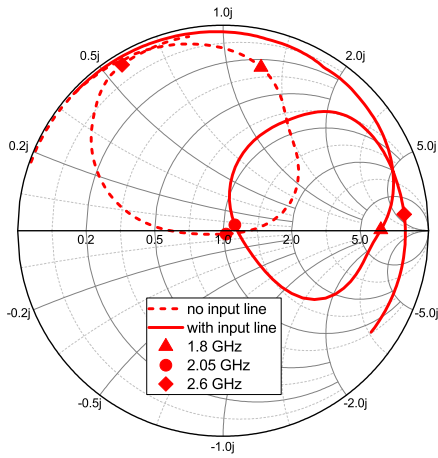
A photograph of the rectifier prototype is shown in Fig. 11.

After a fine-tuning of the value of the lumped components, which has been conducted in order to compensate for additional parasitics not included in the simulations (such as the soldering effects on the paper and the glue of the copper tape, the connectors impact, and so on), the performance of the rectifier under a single tone sweep has been evaluated for different power levels, and the results are reported in Figs. 12–19.

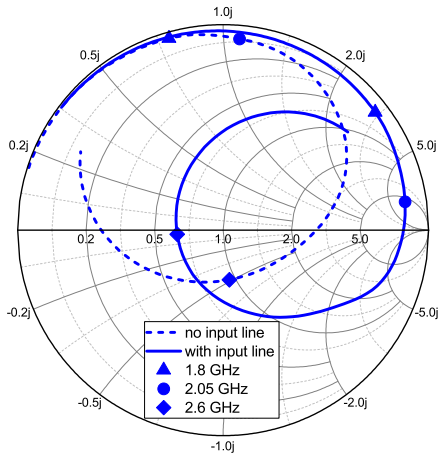
Fig. 12 shows the adequate large signal input reflection coefficient at both ports of the rectifier for a $-15\ \text{dBm}$ available input power. An $|S_{11}|$ value of less than $-6\ \text{dB}$ was achieved throughout all bands of interest.



(a)



(b)



(c)

Fig. 9. Study of rectifier n.2: input reflection coefficient of each branch [(a) B1, (b) B2, and (c) B3] with and without transmission line sections. The simulation results are reported for an available input power of -15 dBm.

In Fig. 13, the rectifier performance in terms of output dc voltage is demonstrated, whereas Fig. 14 shows the resulting RF-to-dc conversion efficiency, which has been derived from

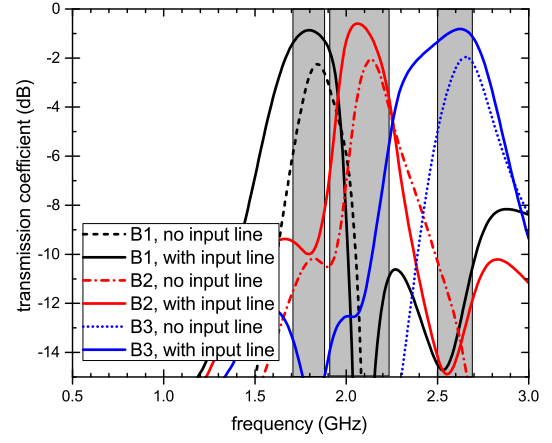


Fig. 10. Transmission coefficient for each branch of rectifier n.2 with and without transmission line sections. The simulation results are reported for an available input power of -15 dBm.

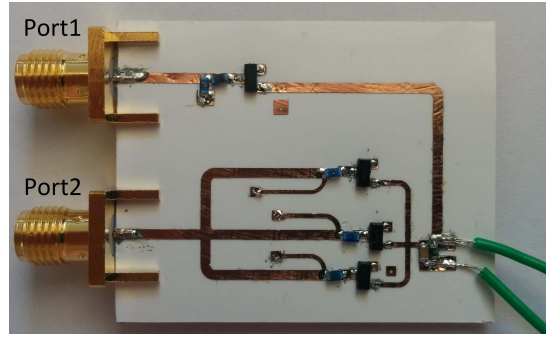


Fig. 11. Photograph of the rectifier prototype. Active area: 3.5×3 cm².

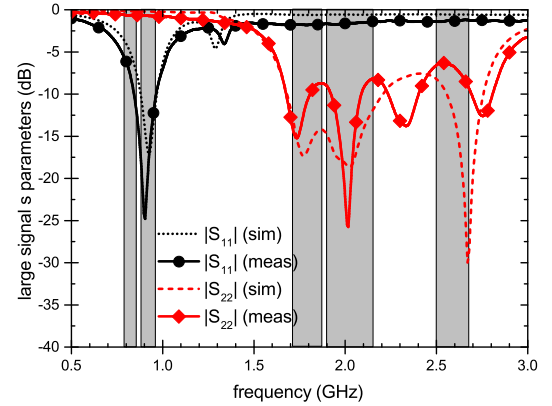
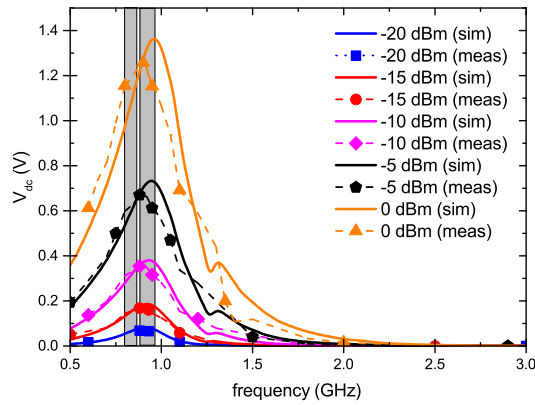


Fig. 12. Rectifier input reflection coefficient for -15 -dBm available input power: comparison between simulations and measurements.

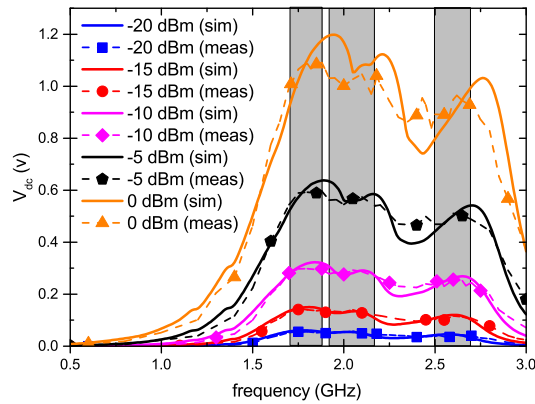
the measured voltage according to

$$\eta_{\text{RF-dc}} = \frac{V_{\text{dc}}^2 / R_L}{P_{\text{avs}}} \times 100 \quad (1)$$

where R_L is the load resistance, V_{dc}^2 / R_L represents the dc power delivered to the load, and P_{avs} is the available RF power at the source. The measurement has been separately carried out for Port1 [reported in Fig. 14(a)] and for Port2 [in Fig. 14(b)].



(a)



(b)

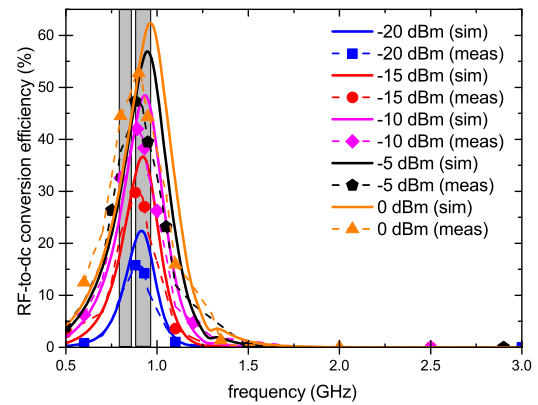
Fig. 13. Multiband rectifier: output dc voltage for a single tone sweep. (a) Port1. (b) Port2.

The first rectifier, which features the best performance, shows an output dc voltage in the operating band ranging from 50 to 70 mV and from 140 to 170 mV for the available input power levels of -20 and -15 dBm, respectively, corresponding to the peak efficiencies of 16% and 30%. Moreover, its peak efficiency grows up to the 52% at 0 dBm.

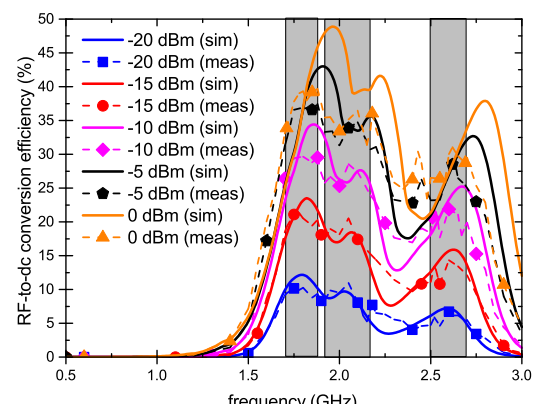
On the other hand, the second rectifier presents an output dc voltage in the range of 36–57 mV and 101–142 mV at -20 and -15 dBm, with the respective peak efficiencies of 10.2% and 21.3%, which are achieved in the first band (band 3 of Table I). In the other two bands, the respective peak efficiencies of 11% and 6% are obtained for -20 dBm and of 20.5% and 14.3% for -15 dBm. This performance deterioration is mainly due to the diode losses, which increase with frequency [32], and to the input interaction and interference among the three branches, which is missing, instead, in the first rectifier.

However, it is worth noticing that the circuit performance varies quite smoothly in all bands for all power levels under test, thus achieving the goal to ensure energy harvesting from all bands of interest.

In Fig. 15, an analysis of the losses associated with both the substrate and the chosen architecture is reported. Four simulations regarding four different scenarios are considered. In the first one, all branches are separated at the input, and the source is connected to one branch at a time, while the others



(a)



(b)

Fig. 14. Multiband rectifier: RF-to-dc conversion efficiency for a single tone sweep. (a) Port1 and (b) Port2.

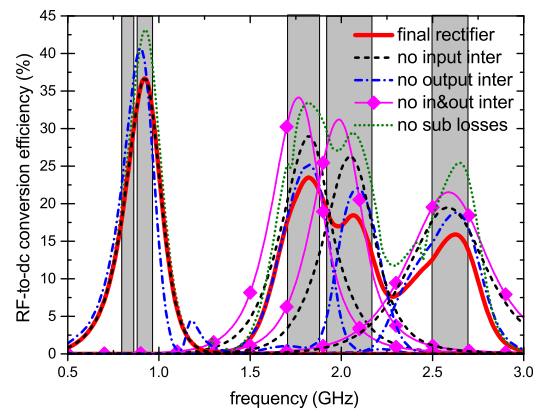


Fig. 15. Multiband rectifier: simulation study of the impact of substrate losses, input and output interactions.

are connected to a $50\text{-}\Omega$ impedance, thus removing the effect of input coupling; in the second one, all rectifier branches are connected to a different output RC filter, thus removing their output interaction; then, the performance of each branch of the rectifier is separately evaluated, i.e., each branch is connected to a different source and load (no input and output interactions); finally, in the fourth one, the substrate losses have been removed without changing the final circuit topology. As a case study, the RF-to-dc conversion efficiency for an available

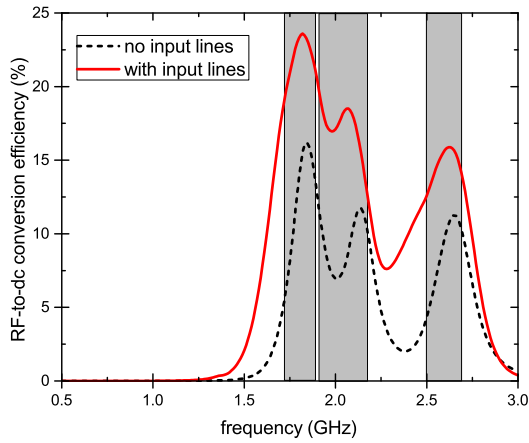


Fig. 16. Simulated RF-to-dc conversion efficiency of rectifier #2 with and without input transmission line sections for an available input power of -15 dBm.

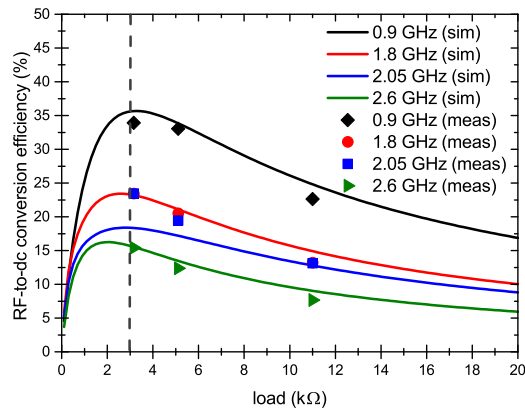


Fig. 17. Multiband rectifier: RF-to-dc conversion efficiency versus load ($P_{avs} = -15$ dBm).

input power of -15 dBm is considered. It is apparent that the major limitation to the rectifier efficiency is represented by the substrate losses, which causes an efficiency reduction around 10% at all center bands. The aggregate losses related to the circuit topology with both input and output coupling are on the whole comparable with the dielectric ones, with the input and output interactions having an impact on average around 7% and 3%, respectively. Nevertheless, the maximum efficiency achieved in [19] around 2.4 GHz is intermediate between the ones of the rectifiers operating around 2.05 and 2.6 GHz without any input and output interactions. It is worth noticing that the branch centered around 900 MHz is only affected by an output interaction, thus experiencing a lower efficiency degradation. Additionally, Fig. 16 highlights the beneficial impact of the input transmission line sections on the conversion efficiency of the second rectifier due to the more selective bandpass characteristic experienced by the input signal in each branch. The simulations were carried out for the -15 -dBm available input power and show an improvement of the peak performance in each subband around 7%.

Fig. 17 reports the RF-to-dc conversion efficiency with respect to the load resistance at the design power of -15 dBm. The optimum load is different for the four branches of

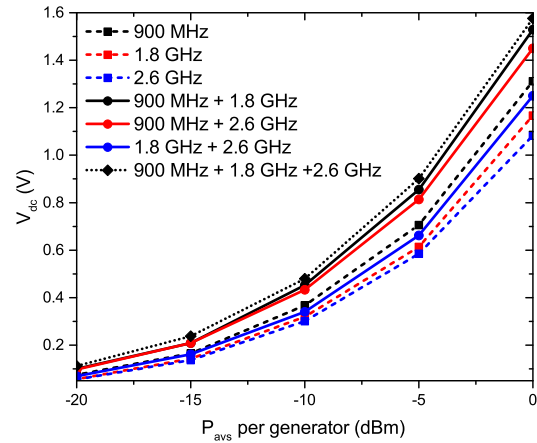


Fig. 18. Multitone test: measured output dc voltage versus an available input power (P_{avs}) per source for one, two, and three tones.

the rectifier, and the value of 3 k Ω is chosen as a result of a tradeoff aimed at maximizing the output dc power under the assumption that an equal amount of power enters each branch of the rectifier at its respective central frequency. This is equivalent to maximizing the sum of the efficiencies calculated at the four central frequencies, as reported in

$$\begin{aligned} P_{dc} &= P_{dc,0.9} + P_{dc,1.8} + P_{dc,2.05} + P_{dc,2.6} \\ &= \eta_{0.9} P_{avs} + \eta_{1.8} P_{avs} + \eta_{2.05} P_{avs} + \eta_{2.6} P_{avs} \\ &= P_{avs} (\eta_{0.9} + \eta_{1.8} + \eta_{2.05} + \eta_{2.6}) \end{aligned} \quad (2)$$

where P_{dc} is the total output dc power, $P_{dc,x}$ is the output dc power corresponding to an RF input power P_{avs} at a frequency of x GHz, and η_x is the RF-to-dc conversion efficiency associated with the P_{avs} input power and calculated at a frequency of x GHz. Therefore, this approach penalizes the rectifier efficiency at 2.6 GHz, which features a maximum efficiency for a load equal to 2 k Ω .

Finally, the circuit performance under multitone input signals has been tested. The rectifier has been connected to three different power generators, each of them transmitting a single tone tuned to 900 MHz, 1.8 GHz, and 2.6 GHz, respectively. The output dc voltage is recorded as a function of the available input power per source for one, two, and three tones. In this way, the rectifier capability to take advantage of the simultaneous presence of multiple tones has been verified. As a second experiment, the power associated with each tone has been randomly varied in such a way that their sum takes values within the range $[-15, -5]$ dBm. This operation has been repeated for 100 times, and the output dc voltage has been recorded with results shown in Fig. 19. It is worth noticing that the data variance is mainly due to the different conversion efficiencies experienced in each band and that, as expected, the best performance is obtained for the lower band. A few points are above the 900-MHz one-tone performance due to the fact that the phases of the three independent generators are randomly combined to achieve an optimized waveform [34].

VI. RF HARVESTER MEASUREMENTS

In order to validate the proposed architecture, the whole rectenna topology was fabricated on a paper substrate, by using

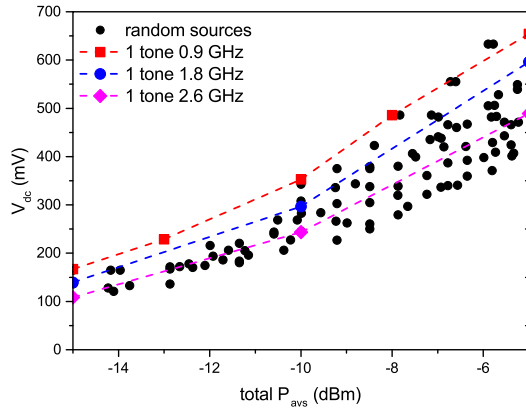


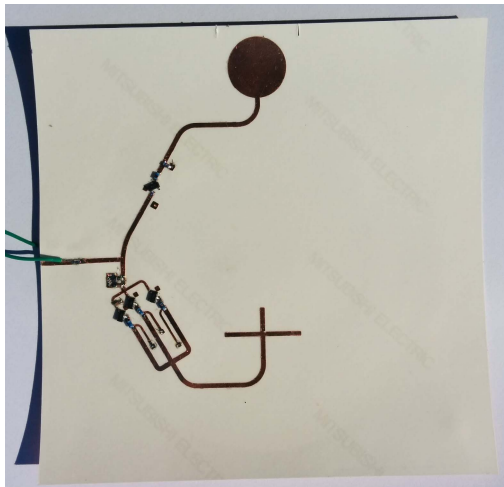
Fig. 19. Multitone test: measured output dc voltage for an available RF input power randomly distributed over three tones.



Fig. 21. Test of the rectenna in laboratory: experimental setup.



(a)



(b)

Fig. 20. Layout of the rectenna prototype. (a) Top side. (b) Bottom side.

the materials and techniques described in Section III, and tested (see Fig. 20 where both sides of the circuit are shown). The rectenna maximum thickness is equal to 1.2 mm, including both the thickness of the substrate and the lumped components. The two rectifiers were arranged so as to take

advantage of the ground plane between the two antennas. This guarantees that the rectifiers are placed near the antenna feed, thus reducing the presence of losses. Moreover, thanks to this arrangement, the rectenna area corresponds to the bare area of the outer antenna, confirming the compactness of the proposed solution, whereas the cut in the outer slot allows for the usage of the outer metal surface to host other circuit components. The proposed rectenna prototype features a weight of only 6 g, while it is conformal and suitable for a broad range of low-cost applications. For instance, it can be used together with a suitable energy storage unit and a circuit with very low duty cycle operation ensuring a large energy autonomy and batteryless operation. Such a system can also be used as a trickle charge for batteries in order to compensate for their self-discharging.

The rectenna performance was first measured in a controlled environment, as reported in Section VI-A, and finally tested in real scenarios, both in normal (flat) and in bent conditions.

A. Rectenna Characterization in a Controlled Environment

A controlled experiment was performed in a laboratory room using the setup shown in Fig. 21. A power source was connected to a double-ridged waveguide horn antenna (3115 model from ETS-LINDGREN). The rectenna was aligned with the antenna and placed at a distance of 1.6 m, which is outside the Fraunhofer region, delimited by the well-known equation (3), for both the transmitting and the receiving antenna

$$R = \frac{2D^2}{\lambda_0} \quad (3)$$

where R is the distance between the phase center of the antennas, D is the largest dimension of the power-source antenna (equal to 25 cm for the horn), and λ_0 is the free-space wavelength associated with the operating frequency.

The rectenna was connected to a multimeter, and the power source was set to three different frequencies (900 MHz, 1.8 GHz, and 2.6 GHz), while for each tone the transmitted power was varied from 5 to 29 dBm. Fig. 22(a) and (b) shows the measured output dc voltage and RF-to-dc conversion efficiency as a function of the power density at the antenna

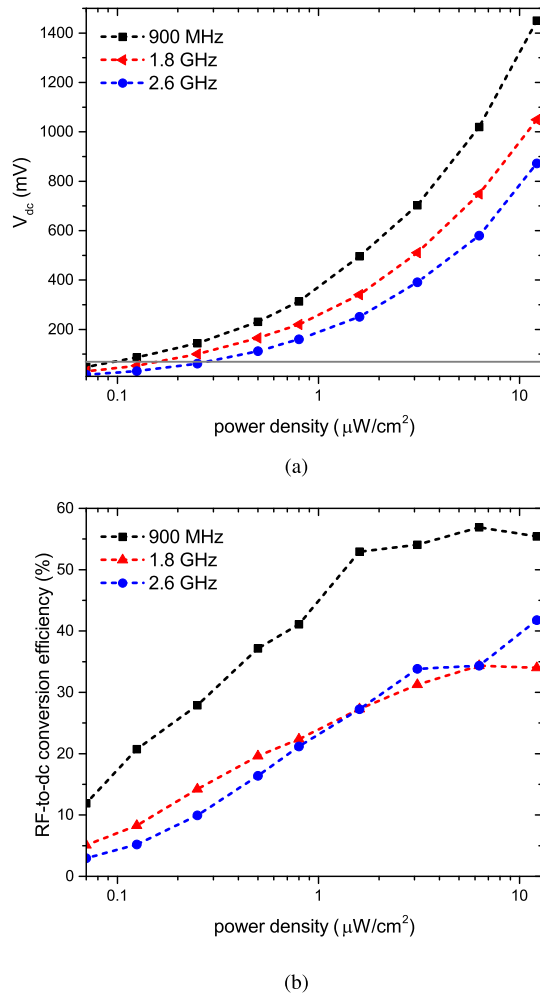


Fig. 22. Test of the rectenna in laboratory. (a) Output dc voltage and (b) RF-to-dc conversion efficiency versus power density. Gray solid line: activation voltage threshold of the state-of-the-art dc/dc converters.

of the harvester. To calculate the latter quantity, the “stand-alone” antenna topology on paper was placed in the same position as the rectenna under test, and it was connected to a power meter. The measured RF input power was divided by the effective area of the respective slot antenna, estimated with the well-known equation as

$$A_{\text{eff}} = G_i \frac{\lambda_0^2}{4\pi} \quad (4)$$

where G_i is the measured gain for the respective-to-the-band slot antenna. In particular, the power density was calculated for the three frequencies of interest for each power level, and the results were averaged in order to compensate for uncertainties stemming from the experimental setup.

According to the obtained results, a power density in the order of 0.1–1 $\mu\text{W}/\text{cm}^2$ is sufficient to activate emerging ultralow voltage electronics, while 10 $\mu\text{W}/\text{cm}^2$ is required for standard electronics (“switch ON” voltage around and above 1 V).

B. Rectenna Testing in Real Scenarios

The performance of the presented flexible rectenna was tested under different bending conditions (see Fig. 23).

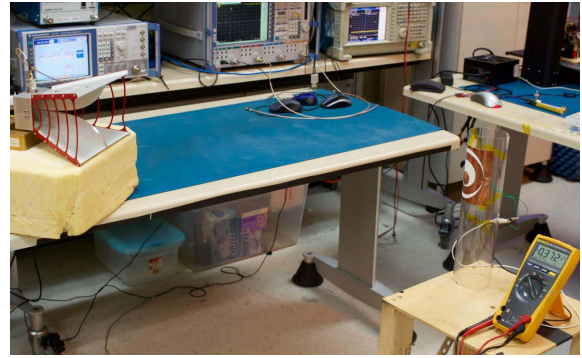


Fig. 23. Rectenna testing under bending conditions: experimental setup.

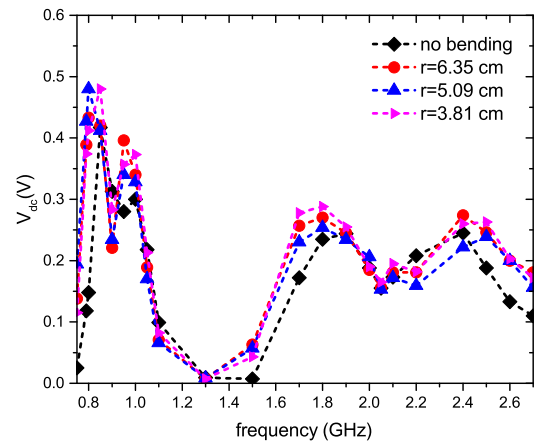


Fig. 24. Rectenna performance under different bending conditions: output dc voltage for different radii of curvature.

The rectenna was placed at a distance of 90 cm and aligned with the transmitting antenna. The latter was connected to a signal generator set to a fixed transmitting power of 15 dBm. The recorded output dc voltages versus frequency were collected for three radii of curvature, as shown in Fig. 24. The impact of bending seems to be neglectable, and the rectenna performance remains nearly unchanged for a radius of curvature as small as 3.81 cm.

The proposed rectenna was proved to be suitable for utilization in a broad range of realistic scenarios, with numerous ambient devices using microwaves for different purposes, thus effectively increasing the local RF power density. For instance, the rectenna was mounted on the door of a microwave oven, which operates at the ISM S-band [Fig. 25(a)]. Despite the power shielding, an output dc voltage around 1 V was measured across the 3-k Ω load during the whole cooking time. In the second example, the rectenna was placed under a smartphone. During an incoming call (GSM900 band), an output dc voltage around 300–400 mV was observed.

C. Performance Comparison

In Table II, a comparison of the presented rectenna with other state-of-the-art rectennas fabricated on flexible and/or unconventional substrates is reported. Reference [19] has already been presented in the introduction, and consists of a single annular slot and an envelope detector. A dual-band

TABLE II
COMPARISON WITH STATE-OF-THE-ART RF ENERGY HARVESTERS

Ref.	Freq. (GHz)	power density ($\mu\text{W}/\text{cm}^2$)	Max Eff. (%)	V_{dc} (V)	Area (cm^2)	Substr.	$\tan\delta$	Tech.
this work	0.79-0.96; 1.71-2.69	6	57	1.02	11x11	paper	0.05	copper tape
[19]	2.4-2.5	3	28	0.26	4.9x5.4	paper	0.05	copper tape
[35]	0.8-0.9; 1.8-1.9	0.2	15	/	13x13	PET	0.08	laser etching
[36]	0.9	8	48.6	/	15.5x5.4	PET	/	inkjet
[37]	2.45	3	1.6	0.2	6x4.5	cardboard	0.042	inkjet
[38]	0.86-0.918	14	50	1.42	19x13.9	pile/jeans	0.009/0.023	conductive non-woven fabric
[39]	0.9; 1.75; 2.45	0.7	19	0.13	17x17	pile/Kapton	-/0.002	Global EMC shielding fabric



(a)



(b)

Fig. 25. Photograph of possible practical scenarios for the proposed rectenna: ambient RF energy harvesting from (a) operating microwave oven and (b) cell phone during an incoming call.

rectifier and a single wideband monopole were used in [35], while [36] was based on a class-F rectifier and a direct matching between the antenna and the diode. In [37], a half-wave double monopole antenna and a two diode rectifier were employed, and finally, multilayer wearable rectennas were proposed both in [38] and [39]. Reference [38] relies on a rectangular patch antenna, while [39] is based on a slot-loaded annular ring antenna; both solutions utilize a single-stage full-wave rectifier. As it can be easily observed,

the majority of these papers focus on single-band or even single-frequency harvesters.

The presented rectenna features a very good performance in terms of occupied area and maximum efficiency with respect to incident power density, while it guarantees operation over a broader frequency range over multiple bands.

VII. CONCLUSION

A novel compact multiband rectenna on paper for ambient RF energy harvesting has been introduced in this effort. Both the design procedure and the measurement results have been thoroughly discussed. The rectenna is able to harvest power in all LTE frequency bands at the available input power levels as low as -20 dBm in a variety of practical and conformal scenarios, thus setting the foundation of truly autonomous IoT and smart node configurations.

Future improvements are also possible: the rectifier can be optimized for multitone operation, for instance, by means of the adoption of higher order bandpass filters in each branch of the second rectifier [12]; the applicability of the system can be freed from orientation constraints by developing compact broadband circularly polarized antennas, achievable through the introduction of ad hoc shorts in specific positions of the slot antennas [28].

ACKNOWLEDGMENT

The authors would like to acknowledge the Keysight Technology and Computer Simulation Technology for license donation of the Advanced Design System and Microwave Studio tools.

REFERENCES

- [1] S. Kim *et al.*, "Ambient RF energy-harvesting technologies for self-sustainable standalone wireless sensor platforms," *Proc. IEEE*, vol. 102, no. 11, pp. 1649–1666, Nov. 2014.
- [2] R. Vyas *et al.*, "Inkjet printed, self powered, wireless sensors for environmental, gas, and authentication-based sensing," *IEEE Sensors J.*, vol. 11, no. 12, pp. 3139–3152, Dec. 2011.
- [3] R. J. Vyas, B. B. Cook, Y. Kawahara, and M. M. Tentzeris, "E-WEHP: A batteryless embedded sensor-platform wirelessly powered from ambient digital-TV signals," *IEEE Trans. Microw. Theory Techn.*, vol. 61, no. 6, pp. 2491–2505, Jun. 2013.
- [4] L. Roselli *et al.*, "Review of the present technologies concurrently contributing to the implementation of the Internet of Things (IoT) paradigm: RFID, green electronics, WPT and energy harvesting," in *Proc. IEEE Topical Conf. Wireless Sensors Sensor Netw. (WiSNet)*, Jan. 2015, pp. 1–3.

- [5] H. Gao, W. Ejaz, and M. Jo, "Cooperative wireless energy harvesting and spectrum sharing in 5G networks," *IEEE Access*, vol. 4, pp. 3647–3658, 2016.
- [6] S. Hanson *et al.*, "Exploring variability and performance in a sub-200-mV processor," *IEEE J. Solid-State Circuits*, vol. 43, no. 4, pp. 881–891, Apr. 2008.
- [7] S. Bandyopadhyay, P. P. Mercier, A. C. Lysaght, K. M. Stankovic, and A. P. Chandrakasan, "A 1.1 nW energy-harvesting system with 544 pW quiescent power for next-generation implants," *IEEE J. Solid-State Circuits*, vol. 49, no. 12, pp. 2812–2824, Dec. 2014.
- [8] V. Marian, C. Menudier, M. Thevenot, C. Vollaïre, J. Verdier, and B. Allard, "Efficient design of rectifying antennas for low power detection," in *IEEE MTT-S Int. Microw. Symp. Dig.*, Jun. 2011, pp. 1–4.
- [9] J. A. Hagerty, F. B. Helmbrecht, W. H. McCalpin, R. Zane, and Z. B. Popovic, "Recycling ambient microwave energy with broad-band rectenna arrays," *IEEE Trans. Microw. Theory Techn.*, vol. 52, no. 3, pp. 1014–1024, Mar. 2004.
- [10] D. Masotti, A. Costanzo, M. D. Prete, and V. Rizzoli, "Genetic-based design of a tetra-band high-efficiency radio-frequency energy harvesting system," *IET Microw. Antennas Propag.*, vol. 7, no. 15, pp. 1254–1263, 2013.
- [11] V. Rizzoli, G. Bichicchi, A. Costanzo, F. Donzelli, and D. Masotti, "CAD of multi-resonator rectenna for micro-power generation," in *Proc. Eur. Microw. Conf. (EuMC)*, 2009, pp. 1684–1687.
- [12] V. Kuhn *et al.*, "A multi-band stacked RF energy harvester with RF-to-DC efficiency up to 84%," *IEEE Trans. Microw. Theory Techn.*, vol. 63, no. 5, pp. 1768–1778, May 2015.
- [13] M. Pinuela, P. D. Mitcheson, and S. Lucyszyn, "Ambient RF energy harvesting in urban and semi-urban environments," *IEEE Trans. Microw. Theory Techn.*, vol. 61, no. 7, pp. 2715–2726, Jul. 2013.
- [14] R. Bergès, L. Fadel, L. Oyhenart, V. Vigneras, and T. Taris, "A dual band 915 MHz/2.44 GHz RF energy harvester," in *Proc. Eur. Microw. Conf. (EuMC)*, Sep. 2015, pp. 307–310.
- [15] H. Sun, Y.-X. Guo, M. He, and Z. Zhong, "A dual-band rectenna using broadband Yagi antenna array for ambient RF power harvesting," *IEEE Antennas Wireless Propag. Lett.*, vol. 12, pp. 918–921, 2013.
- [16] F. Bolos, D. Belo, and A. Georgiadis, "A UHF rectifier with one octave bandwidth based on a non-uniform transmission line," in *IEEE MTT-S Int. Microw. Symp. Dig.*, May 2016, pp. 1–3.
- [17] Z. Liu, Z. Zhong, and Y.-X. Guo, "Enhanced dual-band ambient RF energy harvesting with ultra-wide power range," *IEEE Microw. Wireless Compon. Lett.*, vol. 25, no. 9, pp. 630–632, Sep. 2015.
- [18] V. Palazzi *et al.*, "Design of a ultra-compact low-power rectenna in paper substrate for energy harvesting in the Wi-Fi band," in *Proc. IEEE Wireless Power Transf. Conf. (WPTC)*, May 2016, pp. 1–4.
- [19] V. Palazzi *et al.*, "Performance analysis of a ultra-compact low-power rectenna in paper substrate for RF energy harvesting," in *Proc. IEEE Topical Conf. Wireless Sensors Sensor Netw. (WisNet)*, Jan. 2017, pp. 65–68.
- [20] LTE; Evolved Universal Terrestrial Radio Access (E-UTRA); User Equipment (UE) Radio Transmission and Reception (3GPP TS 36.101 Version 12.7.0 Release 12), document ETSI TS 136 101 V12.7.0 (2015-05), 2015. [Online]. Available: http://www.etsi.org/deliver/etsi_ts/136100_136199/136101/12.07.00_60/ts_136101v120700p.pdf
- [21] AWT Global. LTE E-UTRAN, 3GPP Frequency Bands, accessed on Jul. 9, 2017. [Online]. Available: <http://www.awt-global.com/resources/lte-e-utran-bands/>
- [22] F. Alimenti, P. Mezzanotte, M. Dionigi, M. Virili, and L. Roselli, "Microwave circuits in paper substrates exploiting conductive adhesive tapes," *IEEE Microw. Compon. Lett.*, vol. 22, no. 12, pp. 660–662, Dec. 2012.
- [23] V. Subramanian *et al.*, "Progress toward development of all-printed RFID tags: Materials, processes, and devices," *Proc. IEEE*, vol. 93, no. 7, pp. 1330–1338, Jul. 2005.
- [24] A. J. Steckl, "Circuits on cellulose," *IEEE Spectr.*, vol. 50, no. 2, pp. 48–61, Feb. 2013.
- [25] C. Mariotti *et al.*, "Modeling and characterization of copper tape microstrips on paper substrate and application to 24 GHz branch-line couplers," in *Proc. Eur. Microw. Conf. (EuMC)*, Oct. 2013, pp. 794–797.
- [26] V. Palazzi *et al.*, "A novel compact harmonic RFID sensor in paper substrate based on a variable attenuator and nested antennas," in *IEEE MTT-S Int. Microw. Symp. Dig.*, May 2016, pp. 1–4.
- [27] K.-F. Tong, G. Lacotte, and J. Huang, "Wideband single-fed proximity coupled circularly polarised annular slot antenna," *IET Microw. Antennas Propag.*, vol. 4, no. 10, pp. 1451–1455, Oct. 2010.
- [28] H. Morishita, K. Hirasawa, and K. Fujimoto, "Analysis of a cavity-backed annular slot antenna with one point shorted," *IEEE Trans. Antennas Propag.*, vol. 39, no. 10, pp. 1472–1478, Oct. 1991.
- [29] Y.-W. Jang, "Experimental study of wideband printed annular slot antenna with cross-shaped feedline," *Electron. Lett.*, vol. 38, no. 22, pp. 1305–1307, Oct. 2002.
- [30] K. Niotaki, S. Kim, S. Jeong, A. Collado, A. Georgiadis, and M. M. Tentzeris, "A compact dual-band rectenna using slot-loaded dual band folded dipole antenna," *IEEE Antennas Wireless Propag. Lett.*, vol. 12, pp. 1634–1637, 2013.
- [31] B. L. Pham and A.-V. Pham, "Triple bands antenna and high efficiency rectifier design for RF energy harvesting at 900, 1900 and 2400 MHz," in *IEEE MTT-S Int. Microw. Symp. Dig.*, Jun. 2013, pp. 1–3.
- [32] C. H. P. Lorenz, S. Hemour, and K. Wu, "Physical mechanism and theoretical foundation of ambient RF power harvesting using zero-bias diodes," *IEEE Trans. Microw. Theory Techn.*, vol. 64, no. 7, pp. 2146–2158, Jul. 2016.
- [33] V. Palazzi *et al.*, "Low-power frequency doubler in cellulose-based materials for harmonic RFID applications," *IEEE Microw. Wireless Compon. Lett.*, vol. 24, no. 12, pp. 896–898, Dec. 2014.
- [34] C. R. Valenta and G. D. Durgin, "Rectenna performance under power-optimized waveform excitation," in *Proc. IEEE Int. Conf. RFID*, Apr./May 2013, pp. 237–244.
- [35] A. Collado and A. Georgiadis, "Conformal hybrid solar and electromagnetic (EM) energy harvesting rectenna," *IEEE Trans. Circuits Syst. I, Reg. Papers*, vol. 60, no. 8, pp. 2225–2234, Aug. 2013.
- [36] S. Korrhummel, D. G. Kuester, and Z. Popovic, "A harmonically-terminated two-gram low-power rectenna on a flexible substrate," in *Proc. IEEE Wireless Power Transf. (WPT)*, May 2013, pp. 119–122.
- [37] I. Kharrat, P. Xavier, T.-P. Vuong, and G. E. P. Tourtollet, "Compact rectenna design for lossy paper substrate at 2.45 GHz," *Prog. Electromagn. Res. C*, vol. 62, pp. 61–70, 2016, doi: 10.2528/PIERC15093005.
- [38] G. Monti, L. Corchia, and L. Tarricone, "UHF wearable rectenna on textile materials," *IEEE Trans. Antennas Propag.*, vol. 61, no. 7, pp. 3869–3873, Jul. 2013.
- [39] M. Dini *et al.*, "A fully-autonomous integrated RF energy harvesting system for wearable applications," in *Proc. Eur. Microw. Conf. (EuMC)*, 2013, pp. 987–990.



Valentina Palazzi (S'15) received the B.Sc. and M.Sc. degrees (*magna cum laude*) in electronic engineering from the University of Perugia, Perugia, Italy, in 2012 and 2014, respectively, where she is currently pursuing the Ph.D. degree in industrial and information engineering at the High Frequency Electronics Laboratory.

In 2015, she was a Visiting Ph.D. Student with the Tyndall National Institute, Cork, Ireland. In 2016, she spent three weeks with the Centre Tecnològic de Telecomunicacions de Catalunya, Barcelona, Spain, sponsored by the COST action IC1301 Wireless Power Transmission for Sustainable Electronics. In 2016, she joined the Agile Technologies for High-Performance Electromagnetic Novel Applications Research Group, School of Electrical and Computer Engineering, Georgia Institute of Technology, Atlanta, GA, USA, for five months, where she is currently involved in additive manufacturing technologies and flexible electronics. Her current research interests include the design of passive transponders with sensing capabilities, radar front ends, wireless power transfer technologies, additive manufacturing processes, and conformal electronics.

Ms. Palazzi is a member of IEEE MTT-S TC-24 RFID Technologies. She was a recipient of the First Place Award of the IEEE MTT-S Student Design Competition on Wireless Energy Harvesting held at the International Microwave Symposium 2016. She was also a recipient of the IEEE MTT-S Graduate Fellowship in 2017.



Jimmy Hester (S'14) received the degree in fundamental chemistry, math, and physics, the degree and M.S. degree in electrical and signal processing engineering (with a major in radio frequency electronics) from ENSEEIHT, INP Toulouse, Toulouse, France, in 2012 and 2014, respectively, and the M.S. degree in electrical and computer engineering from the Georgia Institute of Technology, Atlanta, GA, USA, in 2014, where he is currently pursuing the Ph.D. degree in electrical and computer engineering.

He is currently a Research Assistant with the Agile Technologies for High-Performance Electromagnetic Novel Applications Research Group, Georgia Institute of Technology. He has been developing solutions for the use of carbon nanomaterials and optimized RF structures toward the implementation of inkjet-printed flexible low-cost ubiquitous gas sensors for Internet of Things and smart skin applications. His work covers the entire development process, from the development of inkjet inks, improvement of fabrication methods, sensor component design, high-frequency characterization, and environmental testing to the design, simulation, and fabrication of the RF system embedding the sensor. His current research interests include the interface between radio frequency engineering and material science in the form of flexible electronics technologies and nanotechnologies.



Jo Bito (S'13) received the B.S. degree in electrical and electronic engineering from Okayama University, Okayama, Japan, in 2013, and the M.S. degree in electrical and computer engineering from the Georgia Institute of Technology, Atlanta, GA, USA, in 2016, where he is currently pursuing the Ph.D. degree.

From 2010 to 2011, he was with the University of Illinois Urbana-Champaign, Champaign, IL, USA, where he joined the international programs in engineering (IPENG). He is currently a Research

Assistant with the Agile Technologies for High-Performance Electromagnetic Novel Applications (ATHENA) Research Group, Georgia Institute of Technology. His current research interests include the application of inkjet printing technology for flexible and wearable electronics, RF energy harvesting, and wireless power transfer systems.

Mr. Bito was a recipient of the Japan Student Services Organization Long Term Scholarship beginning in 2013.



Federico Alimenti (S'91-A'97-M'06-SM'09) received the Laurea and Ph.D. degrees in electronic engineering from the University of Perugia, Perugia, Italy, in 1993 and 1997, respectively.

In 1996, he was a Visiting Scientist with the Technical University of Munich, Munich, Germany. From 2011 to 2014, he was a Scientific Coordinator of the ENIAC ARTEMOS Project. In 2014, he was a Visiting Professor with the École Polytechnique Fédérale de Lausanne, Lausanne, Switzerland. Since 2001, he has been with the Department of

Engineering, University of Perugia, where he teaches the class "Microwave Electronics." He holds 2 patents and has co-authored over 200 papers in journals and conferences. His current research interests include microwave-integrated circuit design and electronics on cellulose.

Dr. Alimenti was a recipient of the URSI Young Scientist Award in 1996 and the IET Premium (Best Paper) Award in 2013. He was the TPC Chair of the IEEE Wireless Power Transfer Conference in 2013. He has an h-index of 18 in Google Scholar.



Christos Kalialakis (S'94-M'00-SM'09) received the B.Sc. degree in physics and the M.Sc. degree in telecommunications from the Aristotle University of Thessaloniki, Thessaloniki, Greece, in 1993 and 1995, respectively, the Ph.D. degree in electronic and electrical engineering from the University of Birmingham, Birmingham, U.K., in 1999, and the M.B.A. degree from Hellenic Open University, Patras, Greece, in 2016.

He has industry experience in U.K. as an Antenna Designer and then in Greece and USA as an RF Hardware Engineer. Since 2002, he has been with the National Regulatory Authority of Greece for ICT as an Expert on Wireless Communications. He joined the Centre Tecnològic de Telecomunicacions de Catalunya, Barcelona, Spain, in 2015, as a Senior Researcher.



Ana Collado (M'08-SM'12) received the M.Sc. and Ph.D. degrees in telecommunications engineering from the University of Cantabria, Santander, Spain, in 2002 and 2007, respectively.

From 2007 to 2016, she was a Senior Research Associate and the Project Management Coordinator with the Centre Tecnològic de Telecomunicacions de Catalunya, Barcelona, Spain. Since 2016, she has been an Assistant Professor with the Microwaves and Antennas Research Group, School of Engineering and Physical Sciences, Heriot-Watt University,

Edinburgh, U.K. She has participated in national and international research projects. Among her activities, she has collaborated in the organization of several international workshops in different countries of the European Union and also a Training School for Ph.D. students. She has co-authored over 90 papers in journals and conferences. Her current research interests include active antennas, substrate-integrated waveguide structures, nonlinear circuit design, and energy harvesting and wireless power transmission solutions for self-sustainable and energy-efficient systems.

Dr. Collado is a member of IEEE MTT-26 Wireless Energy Transfer and Conversion and MTT-24 RFID Technologies. She serves on the Editorial Board of the *Radioengineering Journal*. She is an Associate Editor of *IEEE Microwave Magazine*, an Associate Editor of the *IET Microwaves, Antennas and Propagation Journal*, and a member of the Editorial Board of the *Cambridge Wireless Power Transfer Journal*.



Paolo Mezzanotte (M'12) was born in Perugia, Italy, in 1965. He received the Ph.D. degree from the University of Perugia, Perugia, in 1997.

Since 2007, he has been an Associate Professor with the University of Perugia, where he has been involved in teaching the class "Radiofrequency Engineering." His current research interests include numerical methods and CAD techniques for passive microwave structures, the analysis and design of microwave and millimeter-wave circuits, and the study of advanced technologies, such as LTCC,

RF-MEMS, and microwave circuits printed on green substrates. These research activities are testified by over 100 publications in the most important specialized journals and at the main conferences of the microwave scientific community. His present h-index (ISI journals) is equal to 13.



Apostolos Georgiadis (S'94–M'02–SM'08) was born in Thessaloniki, Greece. He received the B.S. degree in physics and M.S. degree in telecommunications from the Aristotle University of Thessaloniki, Thessaloniki, in 1993 and 1996, respectively, and the Ph.D. degree in electrical engineering from the University of Massachusetts at Amherst, Amherst, MA, USA, in 2002.

In 2006, he was a Consultant with Bitwave Semiconductor, Lowell, MA, USA. In addition, he collaborated with ACORDE S.A., Santander, Spain, where he was involved in the design of integrated CMOS VCOs for ultrawideband applications. From 2013 to 2016, he was a Group Leader with the Microwave Systems and Nanotechnology Department, Centre Tecnològic de Telecomunicacions de Catalunya (CTTC), Barcelona, Spain. In 2002, he joined Global Communications Devices, North Andover, MA, USA, as a Systems Engineer, where he is involved in CMOS transceivers for wireless network applications. In 2003, he joined Bermai, Inc., Minnetonka, MN, USA, as an RF/Analog Systems Architect. In 2005, he joined the University of Cantabria, Santander, as a Juan de la Cierva Fellow Researcher. In 2007, he joined CTTC as a Senior Researcher in communications subsystems. In 2016, he joined Heriot-Watt University, Edinburgh, U.K., as an Associate Professor. He has authored over 170 papers in peer-reviewed journals and international conferences. His current research interests include energy harvesting and wireless power transmission, RFID technology, active antennas and phased array antennas, inkjet and 3-D printed electronics, and millimeter wave systems.

Dr. Georgiadis is an EU Marie Curie Global Fellow. He is a member of the IEEE MTT-S TC-24 RFID Technologies (past Chair) and a member of the IEEE MTT-S TC-26 Wireless Energy Transfer and Conversion. In 1996, he was the recipient of the Fulbright Scholarship for graduate studies at the University of Massachusetts at Amherst. In 2016, his proposal for Inkjet/3D printed millimeter-wave systems received the Bell Labs Prize, Third Place among more than 250 proposals recognizing ideas that change the game in the field of information and communications technologies. He was the General Chair of the 2011 IEEE RFID-TA Conference and a General Co-Chair of the 2011 IEEE MTT-S IMWS on Millimeter Wave Integration Technologies. He is a Vice Chair of URSI Commission D, Electronics and Photonics and an AdCom member of the IEEE Council on RFID serving as a Vice President of conferences. He is a Distinguished Lecturer of the IEEE Council on RFID. He was an Associate Editor of the *IET Microwaves Antennas and Propagation Journal*, *IEEE MICROWAVE AND WIRELESS COMPONENTS LETTERS*, and the *IEEE RFID VIRTUAL JOURNAL*. He serves as an Associate Editor of the *IEEE JOURNAL ON RFID*. He is the Founder and an Editor-in-Chief of the *Wireless Power Transfer Journal* (Cambridge Univ. Press).



Luca Roselli (M'92–SM'01) joined the University of Perugia, Perugia, Italy, in 1991. In 2000, he founded the spin-off WiS Srl. He was involved in electronic technologies for Internet of Things for six years. He is currently a Qualified Full Professor with the University of Perugia, where he teaches applied electronics and coordinates the High Frequency Electronics Laboratory. He has authored over 280 papers (H-i 23, i10 51, over 2200 citations-Scholar) and *Green RFID System* (Cambridge Univ. Press, 2014). His current research interests include

HF electronic systems with a special attention to RFID, new materials, and wireless power transfer.

Dr. Roselli was a member of the Board of Directors of ART Srl, Urbino, Italy, from 2008 to 2012. He is a member of the list of experts of the Italian Ministry of Research, the past Chair of the IEEE Technical Committees MTT-24-RFID, the Vice Chair of 25-RF Nanotechnologies, 26-Wireless Power Transfer, the ERC Panel PE7, and the Advisory Committee of the IEEE-WPTC, and the Chairman of the SC-32 of IMS. He is the Co-Chair of the IEEE Wireless Sensor Network Conference. He organized the VII Computational Electromagnetic Time Domain in 2007 and the first IEEE Wireless Power Transfer Conference in 2013. He is an Associate Editor of *IEEE Microwave Magazine*. He is involved on the boards of several international conferences. He is a Reviewer for many international reviews, including the PROCEEDINGS OF THE IEEE, the IEEE TRANSACTIONS ON MICROWAVE THEORY AND TECHNIQUES, and IEEE MICROWAVE AND WIRELESS COMPONENTS LETTERS.



Manos M. Tentzeris (S'94–M'98–SM'03–F'10) received the Diploma (*magna cum laude*) degree in electrical and computer engineering from the National Technical University of Athens, Athens, Greece, and the M.S. and Ph.D. degrees in electrical engineering and computer science from the University of Michigan, Ann Arbor, MI, USA.

He was a Visiting Professor with the Technical University of Munich, Munich, Germany, in 2002, he was a Visiting Professor with GTRI-Ireland, Athlone, Ireland, in 2009, and a Visiting Professor with LAAS-CNRS, Toulouse, France, in 2010. He has given over 100 invited talks to various universities and companies all over the world. He has helped develop academic programs in 3-D/inkjet-printed RF electronics and modules, flexible electronics, origami and morphing electromagnetics, highly integrated/multilayer packaging for RF and wireless applications using ceramic and organic flexible materials, paper-based RFID's and sensors, wireless sensors and biosensors, wearable electronics, green electronics, energy harvesting and wireless power transfer, nanotechnology applications in RF, microwave MEMS, and SOP-integrated (ultra-wideband, multiband, mmW, and conformal) antennas, and heads the Agile Technologies for High-Performance Electromagnetic Novel Applications Research Group, Georgia Institute of Technology, Atlanta, GA, USA (20 researchers). He has served as the Head of the GT-ECE Electromagnetics Technical Interest Group, the Georgia Electronic Design Center Associate Director of the RFID/Sensors Research, the Georgia Tech NSF-Packaging Research Center Associate Director of the RF Research, and the RF Alliance Leader. He is currently a Ken Byers Professor in flexible electronics with the School of Electrical and Computer Engineering, Georgia Institute of Technology. He has authored over 650 papers in refereed journals and conference proceedings, 5 books, and 25 book chapters. He holds 14 patents.

Dr. Tentzeris is a member of the URSI-Commission D, the MTT-15 Committee, and the Technical Chamber of Greece, an Associate Member of EuMA, and a Fellow of the Electromagnetic Academy. He was a recipient/co-recipient of the 2017 Georgia Tech Outstanding Achievement in Research Program Development Award, the 2017 Archimedes IP Salon Gold Medal, the 2016 Bell Labs Award Competition 3rd Prize, the 2015 *IET Microwaves, Antennas and Propagation* Premium Award, the 2014 Georgia Tech ECE Distinguished Faculty Achievement Award, the 2014 IEEE RFID-TA Best Student Paper Award, the 2013 *IET Microwaves, Antennas and Propagation* Premium Award, the 2012 FiDiPro Award in Finland, the iCMG Architecture Award of Excellence, the 2010 IEEE Antennas and Propagation Society Piergiorgio L. E. Uslenghi Letters Prize Paper Award, the 2011 International Workshop on Structural Health Monitoring Best Student Paper Award, the 2010 Georgia Tech Senior Faculty Outstanding Undergraduate Research Mentor Award, the 2009 IEEE TRANSACTIONS ON COMPONENTS AND PACKAGING TECHNOLOGIES Best Paper Award, the 2009 E. T. S. Walton Award from the Irish Science Foundation, the 2007 IEEE APS Symposium Best Student Paper Award, the 2007 IEEE IMS Third Best Student Paper Award, the 2007 ISAP 2007 Poster Presentation Award, the 2006 IEEE MTT Outstanding Young Engineer Award, the 2006 Asian-Pacific Microwave Conference Award, the 2004 IEEE TRANSACTIONS ON ADVANCED PACKAGING Commendable Paper Award, the 2003 NASA Godfrey Art Anzic Collaborative Distinguished Publication Award, the 2003 IBC International Educator of the Year Award, the 2003 IEEE CPMT Outstanding Young Engineer Award, the 2002 International Conference on Microwave and Millimeter-Wave Technology Best Paper Award (Beijing, China), the 2002 Georgia Tech-ECE Outstanding Junior Faculty Award, the 2001 ACES Conference Best Paper Award, and the 2000 NSF CAREER Award and the 1997 Best Paper Award from the International Hybrid Microelectronics and Packaging Society. He was the TPC Chair of the IEEE MTT-S IMS 2008 Symposium and the Chair of the 2005 IEEE CEM-TD Workshop. He is the Vice Chair of the RF Technical Committee (TC16) of the IEEE CPMT Society. He is the Founder and the Chair of the RFID Technical Committee (TC24) of the IEEE MTT-S and the Secretary/Treasurer of the IEEE C-RFID. He served as the IEEE MTT-S Distinguished Microwave Lecturer from 2010 to 2012 and the IEEE CRFID Distinguished Lecturer. He is an Associate Editor of the IEEE TRANSACTIONS ON MICROWAVE THEORY AND TECHNIQUES, the IEEE TRANSACTIONS ON ADVANCED PACKAGING, and the *International Journal on Antennas and Propagation*.